KSME

Springer

Journal of Mechanical Science and Technology 38 (6) 2024

Original Article
DOI 10.1007/s12206-024-0523-0

Keywords:
· Cohesive-zone law
· Finite element analysis
· Multi-element interaction
· Roll transfer process
· Rate-dependent adhesion

Correspondence to:
Hyoungsoon Lee
leeh@cau.ac.kr;
Seung Tae Choi
stchoi@cau.ac.kr

Citation:
Her, N., Park, S.-Y., Woo, S., Lee, H., Choi, S. T. (2024). Viscoelastic finite element analysis of roll transfer process with rate-dependent adhesion behavior and multi-element cohesive interaction. Journal of Mechanical Science and Technology 38 (6) (2024) 3039~3046. http://doi.org/10.1007/s12206-024-0523-0

Received January 3rd, 2024
Revised February 12th, 2024
Accepted February 21st, 2024

† Recommended by Editor Hyun-Gyu Kim

Viscoelastic finite element analysis of roll transfer process with rate-dependent adhesion behavior and multi-element cohesive interaction

Namhun Her[1], Si-Young Park[2], Sungwoong Woo[1], Hyoungsoon Lee[1] and Seung Tae Choi[1]

[1]School of Mechanical Engineering, Chung-Ang University, Seoul 06974, Republic of Korea, [2]Molding & Design Solution Team, LG Chem Co., 211 Hwangsar-Ro, Osan-Si, Gyeonggi-Do 18126, Republic of Korea

Abstract In this study, we introduced a multi-element cohesive interaction (MECI) approach for viscoelastic finite element analysis (FEA) to simulate roll transfer processes that involve the rate-dependent adhesion of elastomeric materials, such as polydimethylsiloxane. Viscoelastic FEA focused on transferability of rigid devices from a rigid substrate to a flexible substrate with a silicone elastomer coating. The model incorporated a time-dependent cohesive-zone law (CZL) to represent the rate-dependent characteristics of adhesion between the silicone elastomer and the device. Viscoelastic FEA incorporated adhesive bonding and debonding behaviors with cohesive elements governed by an exponential-type CZL. To address the potential loss of cohesive interaction during slip between contact pairs, we introduced a MECI approach along the contact pairs. We analyzed the effect of rate-dependent adhesion and geometric dimensions on the roll transfer processes. This comprehensive analysis provides insights into the intricate interplay among these factors, contributing valuable knowledge to the understanding of dynamic bonding and debonding processes involving rate-dependent adhesion.

1. Introduction

With recent advancements in flexible electronics, various printing and transfer processes have emerged, facilitating the production of heterogeneous electronic devices on flexible substrates. This ensures that the devices can be bent, folded, or stretched without compromising functionality [1-7]. For example, light emitting diodes can be fabricated on a sapphire wafer and then transferred onto a flexible polyimide substrate through a transfer process [8]. During the transfer process of these heterogeneous devices, they undergo various physical changes as they are exfoliated from the original substrate, transferred to the new substrate, and bonded. In addition, elastomers such as polydimethylsiloxane (PDMS) not only exhibit viscoelastic behavior but also exhibit time-dependent adhesion. This time-dependent adhesion can be effectively controlled to ensure a successful transfer process. However, it is crucial to recognize that analyzing the contact behavior in these viscoelastic materials introduces complexities.

To address contact problems in finite element analysis (FEA), one approach involves using cohesive elements that are governed by the cohesive-zone law (CZL) [9-17]. Many commercial FEA software packages offer standard CZLs, while implementing a complex or unique CZL, such as a rate-dependent CZL [17], requires the use of a user subroutine. In FEA, a CZL, that is, a traction-separation relationship, is implemented between the elements or faces on two corresponding surfaces. Park and Paulino [9] provided a critical review on various cohesive traction-separation relationships and their limitations, especially for mixed-mode problems. In the roll transfer process, the slip phenomenon between devices and a base material is prevalent. When surfaces in contact experience relative motion, such as sliding, the elements constituting the contact pairs change, posing challenges in seamlessly applying the CZL. Therefore, modifications to conventional FEA are necessary to properly analyze this complex phenomenon.

Mai et al. [17] measured the time-dependent CZL between a flat diamond tip and a PDMS film, for which the CZL proposed by Xu and Needleman [13] was modified. This assessment was achieved through flat-tip indentation experiments and viscoelastic FEA. Nanoindentation, employing a flat diamond tip on a PDMS film, was followed by an analysis of the results using the extended Kendall's theory of adhesion [18]. Subsequently, viscoelastic FEA, incorporating cohesive elements, was performed to scrutinize the outcomes of the indentation experiments. The viscoelastic FEA yielded CZLs between the flat tip and PDMS film, contingent upon the time-dependent variables observed during the indentation experiments.

This study employs a user subroutine to implement cohesive elements featuring exponential-type CZLs to analyze bonding and debonding behavior, encompassing surface slippage with time-dependent adhesion energy [13]. To account for slippage, the objective is to establish an element that interacts with multiple elements on the corresponding surface, rather than each element affecting only one of its mates. Using multiple cohesive elements on the surface results in the traction-separation relationship acting on the surface being the summation of the traction-separation relationships of all connected elements. Therefore, when two contacting surfaces experience tangential movement, the displacement in the tangential direction increases even in the absence of vertical displacement. In the traction-separation relationship, this manifests as larger tangential traction and smaller vertical traction. Employing cohesive elements with these multi-element interactions enables the simulation of bonding and debonding processes, even when a significant slip occurs between contact pairs.

This study also aims to perform the viscoelastic FEA of the roll transfer process using cohesive elements while accounting for slip (Fig. 1). Given the variable outcome of whether the device is transferred or not, understanding the impact of the process speed, material properties, and geometry of the roll transfer process on the roll transfer characteristics is important. In addition, the objective is to determine the stresses generated on the device during the roll transfer process to evaluate the potential for device failure. This analysis can reveal adverse effects that may significantly affect the productivity of the roll transfer process.

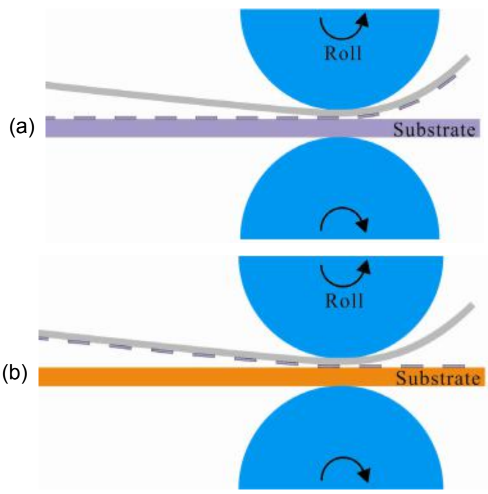

Fig. 1. Typical examples of roll transfer process: (a) roll transfer of devices from a rigid substrate to a flexible film; (b) roll transfer of devices from a flexible film to a rigid substrate.

2. Time-dependent cohesive-zone law

The CZL is a material property employed as a fracture or debonding criterion for materials, such as fracture toughness or critical energy release rate [9-17]. The CZL describes the traction-separation relationship that occurs between two surfaces during the propagation of a crack within a material or the separation of two bonded surfaces. The area beneath the traction-separation curve is equal to the adhesion energy or fracture toughness. In linear elastic fracture mechanics (LEFM), stress is characterized by $1/\sqrt{r}$ singularity around a propagating crack tip. However, the CZL eliminates the singularity of the stress field near the crack tip, proving convenient for FEA.

The exponential form proposed by Xu and Needleman [13] is one of the most widely used mathematical representations of the CZL, expressed as follows:

$$\begin{aligned} T_n = \sigma_{\max} \exp\left(1-\frac{\Delta_n}{\delta_n}\right)\left\{\frac{\Delta_n}{\delta_n}\exp\left(-\frac{\Delta_t^2}{\delta_t^2}\right) \right. \\ \left. +\frac{1-q}{r-1}\left[1-\exp\left(-\frac{\Delta_t^2}{\delta_t^2}\right)\right]\left[r-\frac{\Delta_n}{\delta_n}\right]\right\} + \varsigma_n \frac{d}{dt}\left(\frac{\Delta_n}{\delta_n}\right), \end{aligned} \quad (1)$$

$$\begin{aligned} T_t = 2\sigma_{\max}\left(\frac{\delta_n}{\delta_t}\right)\frac{\Delta_t}{\delta_t}\left[q+\frac{r-q}{r-1}\frac{\Delta_n}{\delta_n}\right]\exp\left(-\frac{\Delta_n}{\delta_n}\right) \\ \times\exp\left(-\frac{\Delta_t^2}{\delta_t^2}\right) + \varsigma_t \frac{d}{dt}\left(\frac{\Delta_t}{\delta_t}\right), \end{aligned} \quad (2)$$

where T_n, T_t, Δ_n, and Δ_t represent normal traction, tangential traction, normal separation and tangential separation, respectively. In addition, $\sigma_{\max}$, δ_n and δ_t denote cohesive strength, characteristic opening displacement, and characteristic shearing displacement, respectively. In addition, the final term in Eqs. (1) and (2) accounts for the fictitious viscous dissipation, which was introduced to mitigate potential numerical instabilities in the FEA of delamination [16]. Here, ς_n and ς_t are variables associated with the fictitious viscous dissipation. The dimensionless number $q = \phi_t / \phi_n$ represents the ratio of the tangential separation energy ϕ_t to the perpendicular separation energy ϕ_n. Another dimensionless number $r = \Delta_n^* / \delta_n$ is the ratio of vertical displacement Δ_n^* to characteristic opening displacement δ_n when pure tangential separation occurs without vertical tension. Figs. 2(a) and (b) illustrate the CZL in the vertical and horizontal directions, respectively, plotted for various parameters.

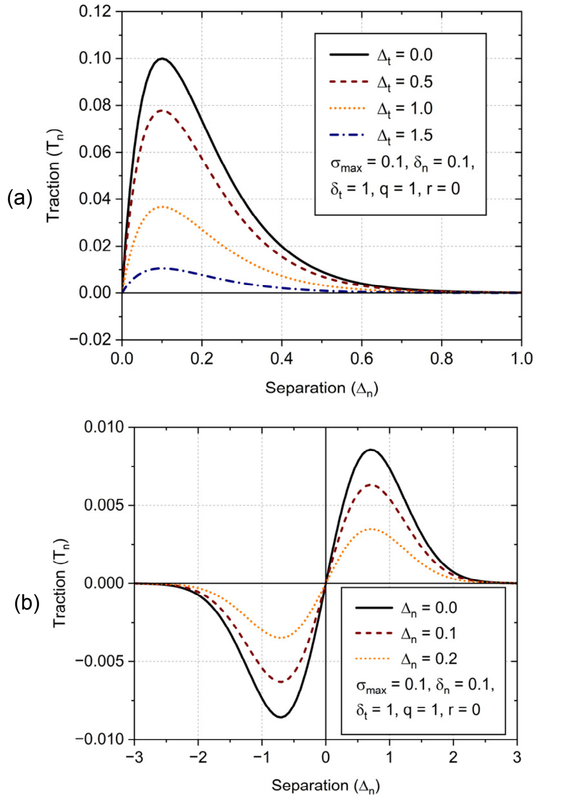

Fig. 2. Traction-separation laws for cohesive elements in the (a) normal direction; (b) tangential direction.

Elastomers, which mechanically exhibit viscoelastic behavior, are also famous for their time-dependent adhesion behavior. Meitl et al. [3] demonstrated the reconstructive use of time-dependent adhesion properties of elastomers in the transfer printing of heterogeneous devices. Mai et al. [17] measured the time-dependent adhesion properties of PDMS, a representative example of elastomers, by indentation test, and obtained the adhesion properties of PDMS using time-dependent CZL as follows:

$$T_n = \sigma_{max}\exp\left(1-\alpha\frac{\Delta_n}{\delta_n}\right)\left\{\frac{\Delta_n}{\delta_n}\exp\left(-\frac{\Delta_t^2}{\delta_t^2}\right) + \frac{1-q}{r-1}\left[1-\exp\left(-\frac{\Delta_t^2}{\delta_t^2}\right)\right]\left[r-\frac{\Delta_n}{\delta_n}\right]\right\} + \varsigma_n\frac{d}{dt}\left(\frac{\Delta_n}{\delta_n}\right). \quad (3)$$

Here, the variable α represents a function of the separation speed Δ_n' given below as follows:

$$\alpha = \alpha_0 + (1-\alpha_0)\exp\left(-\kappa\frac{\Delta_n'}{\delta_0'}\right), \quad (4)$$

where α_0, κ and δ_0' represent the material parameters dependent on the separation rate, and the values for PDMS are given in Table 1 of Mai et al. [17]. For the CZL in the tangential direction, the time-dependent relation from Eq. (2) is employed.

Mai et al. [17] also proposed to take the effect of dwell time into account by expressing the parameter σ_{max} as a function of the contact time t_c as follows:

$$\sigma_{max} = \sigma_0 + \sigma_c\left[1-\exp\left(-\frac{t_c}{t_0}\right)\right], \quad (5)$$

where σ_0 and σ_c are the initial and additional cohesive strengths, respectively, and t_0 is a reference time constant, and the values for PDMS are also given in Table 1 of Mai et al. [17]. However, the dwell time typically is effective for relatively long periods of contact (more than hundreds of seconds), which does not occur in the roll transfer process. Therefore, the effect of dwell time is not considered in this study.

It is well known that rather than the detailed shape of the cohesive-zone law being important, its area provides the adhesion energy and can be obtained by integrating the cohesive traction over the separation according to

$$\gamma_\alpha = \int_0^\infty T_n(\Delta_n)\,d\Delta_n = \frac{e}{\alpha^2}\sigma_{max}\delta_n, \quad (6)$$

where the separation rate is assumed to be constant. Eq. (6) shows the dependence of the adhesion energy on the separation rate and contact time through the parameters given in Eqs. (4) and (5), respectively [17]. It is worth noting that the time-dependent CZL given in Eqs. (2)-(5) with the numerical parameter values given in Table 1 of Mai et al. [17] can be used to simulate the time-dependent adhesive bonding and debonding processes between PDMS and any other materials in the appropriate separation rate and contact time ranges.

3. Viscoelastic finite element analysis

3.1 Surface interaction with multiple cohesive elements

In an FEA with cohesive elements, the traction-separation relationship is enforced between the corresponding elements or faces between two adherends. In this study, the CZL given in Eqs. (2) and (3) for time-dependent normal and tangential traction-separation relations, respectively, is incorporated into the user subroutine of the commercial FEA software, ABAQUS [19]. The CZL can be applied to the mating cohesive elements or mating surfaces of the two adherends. However, it is worth noting that in conventional LEFM, the two adherends are irreversibly separated by cracking or debonding processes and thus do not adhere again. However, adhesive bonding and debonding of elastomeric materials can be repeated multiple times, despite the occurrence of viscoelastic energy dissipation. Therefore, it is crucial to incorporate this feature into the ABAQUS user subroutine. In particular, the cohesive interaction should remain valid even in the presence of a substantial slip

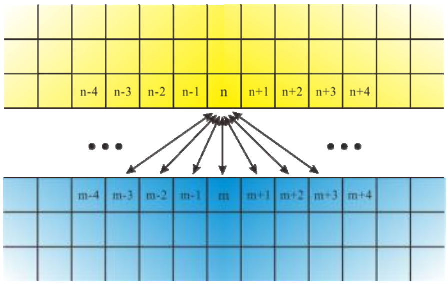

Fig. 3. Schematic illustrations of multiple-element cohesive interactions among finite elements.

between mating cohesive elements, as long as the normal separation between the two adherend surfaces is smaller than the characteristic opening displacement δ_n . In the roll transfer process, frequent occurrences of slip between the device and the base material necessitate consideration in the implementation of the cohesive interaction scheme within the ABAQUS user subroutine.

This study considers the multiple-element cohesive interaction (MECI) with the time-dependent CZL, as illustrated in Fig. 3. Specifically, a cohesive element on one adherend can interact with multiple elements on the other adherend, and vice versa. It is worth noting that in the presence of MECI, the CZL acting on an element is the sum of the traction-separation relationships of all connected elements. The one-to-one traction-separation relationship needs to be revised accordingly. In addition, the MECI may require a more computational time than one-to-one cohesive interaction. Consequently, the optimal number of MECI elements should be selected based on specific conditions involving bonding, debonding, and slip processes. Particularly, in scenarios such as the slip occurring in the roll transfer process, where the two adhesive surfaces move tangentially, the displacement in the tangential direction increases even when the vertical displacement remains constant. Therefore, careful consideration is essential in determining the number of MECI elements from the corresponding one-to-one traction-separation relationship.

3.2 Viscoelastic FEA for roll transfer process

Figs. 1(a) and (b) show typical examples of the roll transfer process [3, 20]: (a) Roll transfer of devices from a rigid substrate to a flexible film, and (b) roll transfer of devices from a flexible film to a rigid substrate, for which viscoelastic FEA is performed in this study. A key aspect of the roll transfer process is to control the time-dependent adhesion of devices and substrates through adjustments in the process speed. In this context, the device to be transferred is a thin Si device bonded to a Si substrate with weak adhesion, and the flexible substrate onto which the device is transferred is a polyethylene terephthalate (PET) film with a thin silicone elastomer coating. The thin silicone elastomer coating is regarded as PDMS. The elastomer coating PDMS exhibits not only viscoelastic behavior but also time-dependent adhesion characteristics. Consequently, a slow process speed decreases the adhesion of the elastomer, whereas fast process speed increases it [17]. Therefore, viscoelastic FEA is performed to analyze the process of separating the Si device from the Si substrate and transferring it to the silicone-coated flexible PET. In this study, ABAQUS Ver. 6.25 (CAE, Standard & Explicit), a commercial FEA program with the UMAT user subroutine, is used to perform FEA with MECI.

Table 1. Geometric parameters and elastic constants of the components used in the FEA [17].

Material	Thickness (μm)/ length (μm)	Young's modulus (MPa)	Poisson's ratio
PET	191/2000	3000	0.38
PDMS	5/2000	1.42	0.48
Silicon device	5/400	150000	0.17
	3/400		
	5/300		
Silicon substrate	50/2000	150000	0.17

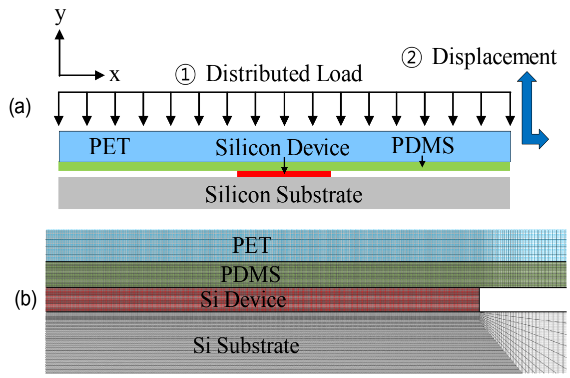

Fig. 4. (a) Schematic geometry of the roll transfer process model, of which the scales and aspect ratios are not the same as the real values; (b) A partial view of the viscoelastic FEA mesh near the silicon device, in which MECI is applied between PDMS and silicon device as well as between PDMS and silicon substrate, for which the time-dependent CZLs given in Eqs. (2) and (3) are used.

The specific geometry used in the viscoelastic FEA is shown in Fig. 4, and the material properties and geometric parameters used in the simulation are listed in Table 1. Choi et al. [21] performed the modified creep experiment with a flat indenter tip and measure the relaxation modulus of PDMS in Prony series, Eq. (10) of Choi et al. [21], which is used in our viscoelastic FEA. The three different sizes (thickness and length) of the Si device are provided in Table 1. The time-dependent CZL is applied between the PDMS coating and the Si devices, while the time-independent CZL is applied between the Si devices and the Si substrate.

The FEA of the roll transfer process is performed in the following three sequential steps (refer to Fig. 4(a)): First, a distributed load is applied to the top of the PET, which simulates the pressure supported by the rollers. Second, the distributed load is removed, indicating the departure of the Si device from the roller region. Third, to illustrate the debonding process, both horizontal and vertical displacement components are applied to the right edge of the flexible PET substrate. This can be considered to be a reasonable boundary conditions when referred to the roll transfer process illustrated in Fig. 1(a). That is, the horizontal component of displacement may cause slip of relative motion, and thus it seems logical to use MECI. On the other hand, the vertical displacement may control the debonding velocity and thus strongly affect the adhesion between the PDMS and the Si device. Fig. 4(b) represents an enlarged view of finite elements near cohesive zones. It is recommended that the element size should be smaller than 0.2 μm to ensure stable FEA of debonding processes with the time-dependent CZL of PDMS [17].

4. Results and discussion

4.1 Three types of the roll transfer process results

The viscoelastic FEA of the roll transfer process with the rate-dependent CZL and MECI is conducted following the methodology outlined in Sec. 3.2, and the typical three types of the results are shown in Fig. 5. Figs. 5(a)-(c) illustrate instances of an unsuccessful transfer, a partial separation, and a successful transfer of the Si device from the substrate, respectively. The unsuccessful transfer (Fig. 5(c)) is an undesirable situation, where the PDMS-Si adhesion is not enough to detach the Si device from the Si substrate. Contrarily, the successful transfer (Fig. 5(a)) is a recommended situation for the roll transfer process, where the PDMS-Si adhesion is enough to detach the Si device from the Si substrate. The partial separation (Fig. 5(b)) represents several situations: (1) both interfaces (PDMS-Si and Si-SI) are partially debonded, (2) the viscoelastic FEA is interrupted by too many equilibrium iterations due to a subtle balance between PDMS-Si adhesion and Si-Si adhesion. The key factor among various parameters affecting the transferability of the Si device, such as the speed, material properties, and geometrical parameters of the roll transfer process, may be the vertical velocity of the flexible substrate (process speed), since it changes the adhesion energy between the Si device and PDMS coating. Therefore, increasing the roll transfer speed may increase the probability of successful transfer of the Si device. In the following section, the effect of the process speed on the transferability is examined in detail.

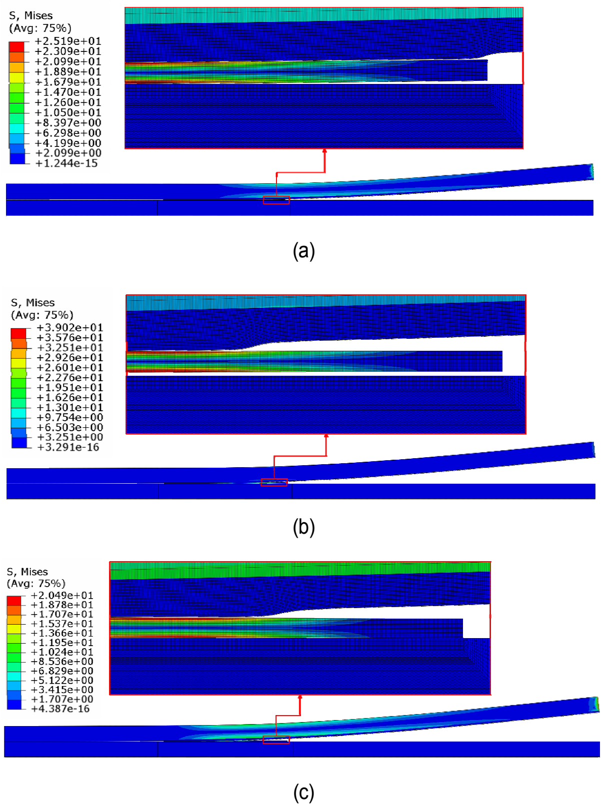

Fig. 5. Three types of roll transfer FEA results: (a) the silicon device is successfully detached from the silicon substrate; (b) the silicon device is partially detached from the silicon substrate; (c) the silicon device is not detached from the silicon substrate.

4.2 Transferability of Si devices and time-dependent adhesion

The transferability of the Si device is determined by the competition between the PDMS-Si adhesion energy and the Si-Si adhesion energy. Notably, the Si-Si adhesion energy is independent of the process speed, whereas the PDMS-Si adhesion energy may increase with higher process speeds. Mai et al. [17] used the time-dependent CZL given in Eqs. (2)-(6) and measured the adhesion between a PDMS film and a flat diamond tip by using the flat indentation experiment. In this study, the time-dependent adhesion between PDMS and diamond measured by Mai et al. [17] is assumed to be the same as that between PDMS and Si device and used in this study to simulate the roll transfer process.

Fig. 6 illustrates the transferability map from a Si substrate to a flexible film of a Si device, as a function of the vertical velocity of the flexible substrate and Si-Si adhesion energy. As anticipated, lower Si-Si adhesion energy and higher vertical velocity of the flexible substrate enhance the efficacy of the transfer process. However, it is imperative to acknowledge that Si-Si adhesion energy represents a material property, while the vertical velocity of the flexible substrate denotes a specific geometric parameter with potential limitations in universal applicability. In this investigation, the vertical velocity of the flexible substrate is delineated with respect to a distance of 1000 μm from the Si device. From a fundamental standpoint, it is more physically justifiable to replace this velocity with the debonding velocity or crack propagation velocity of the polydimethylsiloxane (PDMS)-Si interface, since the time-dependent adhesion behavior of PDMS, characterized by its viscoelastic nature, exhibits a close correlation with energy dissipation, proportionate to crack propagation velocity.

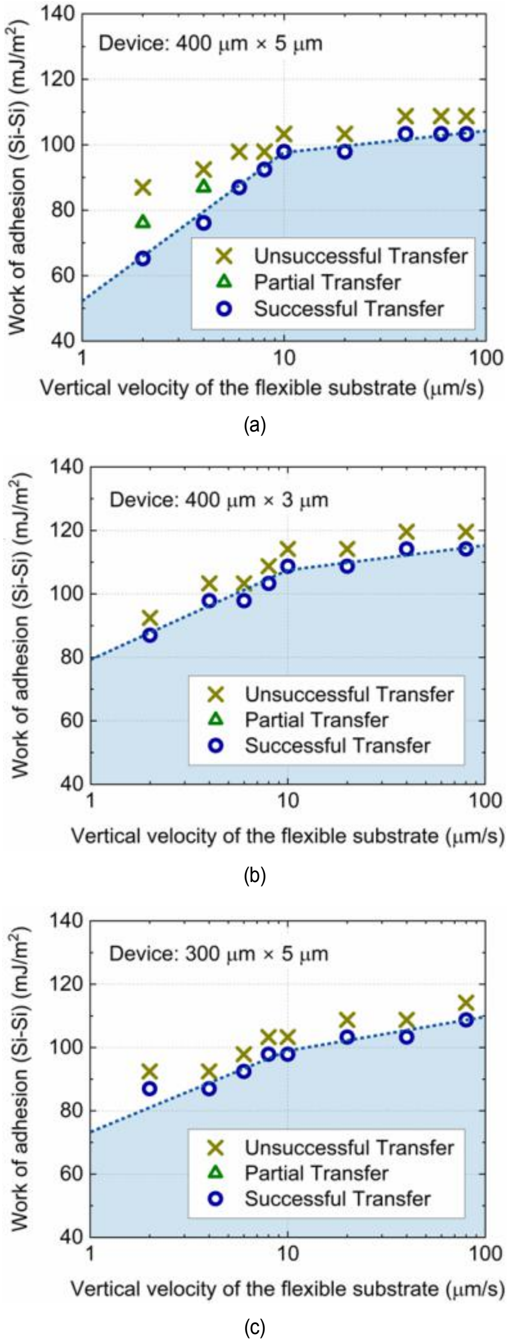

Fig. 6. Maps of successful detachment of a silicon device from a silicon substrate as a function of the adhesion energies between the silicon device and PDMS as well as between the silicon device and the silicon substrate, when the silicon device size is (a) 400 μm × 5 μm; (b) 400 μm × 3 μm; (c) 300 μm × 5 μm.

Figs. 6(a)-(c) present the results of the viscoelastic FEA outlined in Sec. 3.2 for Si device dimensions of 400×5 μm^2, 400×3 μm^2, and 300×5 μm^2, respectively. Across all scenarios, the vertical velocity of the flexible substrate exhibits significant rate-dependence below 10 μm/s, while displaying minimal rate-dependence beyond 10 μm/s. This phenomenon above 10 μm/s can be attributed to the time-dependent adhesion characteristics of PDMS measured by Mai et al. [17]. However, it's worth noting that Mai et al. [17] employed an instrumented indentation method, which may have limited their ability to conduct high-speed experiments. Consequently, obtaining more precise PDMS properties at higher speeds is expected to enhance the accuracy of interpretation.

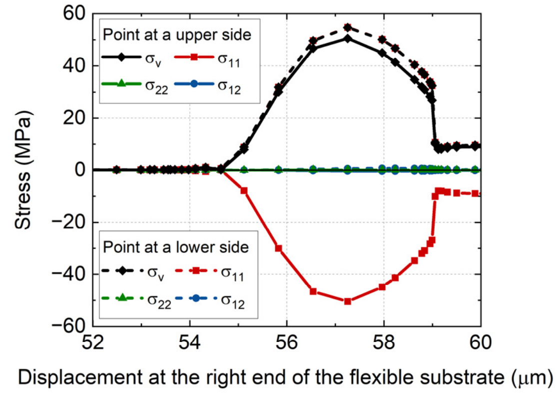

Fig. 7. Stress evolution at upper and lower points of the silicon device as a function of the displacement of the right side of the flexible film, when the silicon device is successfully detached from the silicon substrate.

In comparison to the 400×5 μm^2 device (Fig. 6(a)), the 400×3 μm^2 device (Fig. 6(b)) demonstrates superior transfer performance, despite having a larger Si-Si adhesion energy. This discrepancy arises from the reduction in bending stiffness proportional to the cube of the thickness as the device thickness diminishes. Consequently, the decreased bending stiffness diminishes the cohesive-zone length [22], facilitating the overcoming of the larger adhesion energy (Si-Si) for debonding. In addition, the decrease in length of Si device from 400×5 μm^2 (Fig. 6(a)) to 300×5 μm^2 (Fig. 6(c)) may directly diminish the cohesive-zone length [22] so that the transferability may also increase, enabling the surmounting of the larger adhesion energy (Si-Si) for debonding.

4.3 Stress distribution

In Fig. 7, the stress components, σ_{11}, σ_{22}, σ_{12} and von Mises stress σ_v, within the Si device are plotted as functions of the displacement of the right end of the PDMS/PET flexible substrate. This illustration corresponds to the case in which the Si device is successfully lifted from the Si substrate. The stresses at the points of maximum stress on the top and bottom surfaces of the Si device are plotted. Notably, the stress component σ_{11}, parallel to the device, attains the highest value among the stress components. In addition, the bottom and top surfaces of the device exhibit similar magnitudes of σ_{11} but with opposite signs. This observation indicates that stress primarily arises from bending deformation during the roll transfer process. Notably, when separation occurs between the Si device and the Si substrate during roll transfer, the stress significantly increases.

The bending stress, σ_{11}, generated during the roll transfer

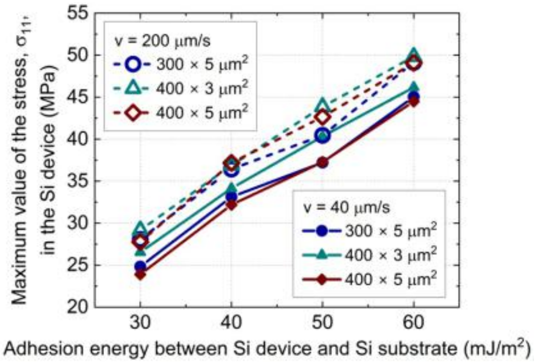

Fig. 8. Maximum stress (σ_{11}) in the silicon device as a function of the adhesion energy between the Si device and the Si substrate.

process may depend on the process speed, Si-Si adhesion energy, and geometric parameters. Fig. 8 shows the largest stress component in the device, σ_{11}, as a function of the Si-Si adhesion energy for different Si device sizes. Obviously, as the Si-Si adhesion energy increases, the maximum value of the bending stress, σ_{11}, almost linearly increases. The length of Si device has no strong effect on the maximum value of the bending stress during the roll transfer process. However, interestingly, among three different Si devices, the thinner device (3 μm thickness) exhibits the highest bending stress representing the largest bending curvature during debonding process. In addition, it is worth noting from Fig. 8 that the higher process speed produces the higher bending stress, since the higher process speed increases the adhesion between PDMS and Si device. It is worth noting that for higher values of Si-Si adhesion energy, the viscoelastic FEA with the time-dependent CZL and MECI cannot be always performed to the complete separation but sometimes only to the middle of separation, and thus, the maximum values of the bending stress σ_{11} cannot be succesfully reported for Si-Si adhesion energy greater than 80 mJ/m^2. However, it is expected that the maximum values of the bending stress, σ_{11}, will increase monotonically in proportion to the Si-Si adhesion energy.

5. Conclusions

In this study, we performed viscoelastic FEA with a time-dependent cohesive-zone law and a multi-element cohesive interaction by using an ABAQUS user subroutine to analyze bonding and debonding behavior, including slip of surfaces. To account for slip, we configured an element to interact with multiple elements on the corresponding surfaces. Employing multiple cohesive elements on a surface results in the traction-separation relation acting on a face being the sum of the traction-separation relations of all connected elements. A viscoelastic FEA of the bonding and debonding between the device and the base material in the roll transfer process was performed using these cohesive elements with multi-element interactions. We analyzed the effects of the process speed, material properties, and geometry on the roll transfer characteristics because the device may or may not be transferred depending on the adhesion energy between the device and the substrate and the adhesion energy between the device and the film (flexible substrate to be transferred). In addition, it is essential to note that the primary stress generating factor during the roll transfer is bending deformation, and we identified the possibility of device failure. The multi-element cohesive interaction scheme with a time-dependent CZL developed in this study is expected to be applicable to various bonding and debonding processes with significant slip.

Acknowledgments

This research was supported by the Chung-Ang University Research Scholarship Grants in 2022 and by the National Research Foundation of Korea (NRF) grant funded by the Korea government (MSIT) (No. 2021R1A2C2094534).

Nomenclature

T_n : Opening-mode traction in a cohesive-zone
T_t : Shearing-mode traction in a cohesive-zone
Δ_n : Opening-mode displacement in a cohesive-zone
Δ_t : Shearing-mode displacement in a cohesive-zone
T_n : Cohesive strength in a cohesive zone
δ_n : Characteristic opening displacement in a cohesive-zone
δ_t : Characteristic shearing displacement in a cohesive-zone
ς_n : Fictitious viscous parameters in the normal direction
ς_t : Fictitious viscous parameters in the tangential direction
ϕ_n : Normal separation energy
ϕ_t : Tangential separation energy

References

[1] S. Bae, H. Kim, Y. Lee, X. Xu, J. Park, Y. Zheng, J. Balakrishnan, T. Lei, H. R. Kim, Y. I. Song, Y. Kim, K. S. Kim, B. Özyilmaz, J. Ahn, B. H. Hong and S. Iijima, Roll-to-roll production of 30-inch graphene films for transparent electrodes, *Nat. Nanotechnol.*, 5 (8) (2010) 574-578.

[2] B. K. Sharma, B. Jang, J. E. Lee, S. Bae, T. W. Kim, H. Lee, J. Kim and J. Ahn, Load-controlled roll transfer of oxide transistors for stretchable electronics, *Adv. Funct. Mater.*, 23 (16) (2013) 2024-2032.

[3] M. A. Meitl, Z. Zhu, V. Kumar, K. J. Lee, X. Feng, Y. Y. Huang, I. Adesida, R. G. Nuzzo and J. A. Rogers, Transfer printing by kinetic control of adhesion to an elastomeric stamp, *Nat. Mater.*, 5 (1) (2006) 33-38.

[4] D. S. Grierson, F. S. Flack, M. G. Lagally and K. T. Turner, Rolling-based direct-transfer printing: a process for large-area transfer of micro- and nanostructures onto flexible substrates, *J. Appl. Phys.*, 120 (9) (2016) 093103.

[5] C. Linghu, S. Zhang, C. Wang and J. Song, Transfer printing techniques for flexible and stretchable inorganic electronics, *NPJ Flex. Electron.*, 2 (1) (2018) 26.

[6] H. Zhou, W. Qin, Q. Yu, H. Cheng, X. Yu and H. Wu, Transfer

printing and its applications in flexible electronic devices, *Nanomater.*, 9 (2) (2019) 283.
[7] J. Bian, L. Zhou, X. Wan, C. Zhu, B. Yang and Y. Huang, Laser transfer, printing, and assembly techniques for flexible electronics, *Adv. Electron. Mater.*, 5 (7) (2019) 1800900.
[8] W. Choi, H. J. Park, S. Park and T. Jeong, Flexible InGaN LEDs on a polyimide substrate fabricated using a simple direct-transfer method, *IEEE Photonics Technol. Lett.,* 26 (21) (2014) 2115-2117.
[9] K. Park and G. H. Paulino, Cohesive zone models: a critical review of traction-separation relationships across fracture surfaces, *Appl. Mech. Rev.*, 64 (6) (2011) 060802.
[10] M. A. Puso and T. A. Laursen, A mortar segment-to-segment frictional contact method for large deformations, *Comput. Methods Appl. Mech. Eng.*, 193 (45-47) (2004) 4891-4913.
[11] E. Lorentz, A mixed interface finite element for cohesive zone models, *Comput. Methods Appl. Mech. Eng.*, 198 (2) (2008) 302-317.
[12] J. Cen and K. Komvopoulos, A cohesive-zone-based contact mechanics analysis of delamination in homogeneous and layered half-spaces subjected to normal and shear surface tractions, *J. Appl. Mech.*, 90 (7) (2023) 071011.
[13] X.–P. Xu and A. Needleman, Numerical simulations of fast crack growth in brittle solids, *J. Mech. Phys. Solids*, 42 (9) (1994) 1397-1434.
[14] M. Elices, G. V. Guinea, J. Gómez and J. Planas, The cohesive zone model: advantages, limitations and challenges, *Eng. Fract. Mech.*, 69 (2) (2002) 137-163.
[15] S. T. Choi and K.-S. Kim, Nanoscale planar field projections of atomic decohesion and slip in crystalline solids. Part I. A crack-tip cohesive zone, *Philos. Mag.*, 87(12) (2007) 1889-1919.
[16] Y. F. Gao and A. F. Bower, A simple technique for avoiding convergence problems in finite element simulations of crack nucleation and growth on cohesive interfaces, *Model. Simul. Mater. Sci. Eng.*, 12 (3) (2004) 453-463.
[17] N. T. Mai, S. T. Choi, K. Chung, S. R. Lee, D. K. Shin and Y. Y. Earmme, Time-dependent adhesion of a polydimethylsiloxane (PDMS) elastomer film to a flat indenter tip characterized using a cohesive-zone law, *Philos. Mag. Lett.*, 94 (4) (2014) 242-250.
[18] K. Kendall, The adhesion and surface energy of elastic solids, *J. Phys. D: Appl. Phys,* 4 (8) (1971) 1186.
[19] Dassault Systèmes Simulia Corp., *ABAQUS User's Manual, Ver. 6.13*, Dassault Systèmes Simulia Corp., Providence, RI, USA.
[20] K. Sohn, J. H. Park, D. Lee, H. Jang and W. I. Lee, Effects of the process temperature and rolling speed on the thermal roll-to-roll imprint lithography of flexible polycarbonate film, *J. Micromech. Microeng.*, 23 (3) (2013) 035024.
[21] S. T. Choi, S. J. Jeong and Y. Y. Earmme, Modified-creep experiment of an elastomer film on a rigid substrate using nanoindentation with a flat-ended cylindrical tip, *Scr. Mater.*, 58 (3) (2008) 199-202.
[22] K. Ha, H. Baek and K. Park, Convergence of fracture process zone size in cohesive zone modeling, *Appl. Math. Model.*, 39 (19) (2015) 5828-5836.

Namhun Her received his B.S. degree in Mechanical Engineering from Chung-Ang University, Seoul, Republic of Korea, in 2022. He is currently a M.S. degree candidate in Chung-Ang University. His current research interests include the fabrication of porous fibers via thermal drawing technique and its application to fiber-based helical actuators.

Si-Young Park received his M.S. degree in Mechanical Engineering from University of Ulsan, Ulsan, Republic of Korea, in 2015. He is currently working for LG Chemical Co. His research interest includes multiphysics simulation of plastic materials, especially under impact loading.

Sungwoong Woo received his B.S. degree in Mechanical Engineering from Kunsan National University, Jeollabuk-do, Republic of Korea, in 2022. He is currently a M.S. degree candidate in Chung-Ang University. His current research interests include piezoresistive insole sensors.

Hyoungsoon Lee is an Associate Professor in the School of Mechanical Engineering at Chung-Ang University, Seoul, Korea. He received his B.S. in Mechanical Engineering from Korea University, Seoul, Korea, in 2006, and went on to complete his M.S. in 2011 and Ph.D. in 2014, both in Mechanical Engineering, from Purdue University. His research interests encompass phase-change heat transfer and thermal management in electronics.

Seung Tae Choi received the B.S. degree in mechanical design and precision engineering from Chung-Ang University, Seoul, Republic of Korea, in 1995, and the M.S. and Ph.D. degrees in mechanical engineering from Korea Advanced Institute of Science and Technology (KAIST), Daejeon, Republic of Korea, in 1997 and 2002, respectively. In 2016, he joined Chung-Ang University, Seoul, Republic of Korea, where he is currently a Professor in the School of Mechanical Engineering. His current research interests include development of multifunctional fibers and ferroelectric polymer sensors and actuators.